38

July 2005

ST-ECF Newsletter

Space Telescope European Coordinating Facility

This picture shows part of the Eagle Nebula (M16), a spectacular nearby region of active star-formation. The image was released to coincide with the 15th Anniverary of the Hubble Space Telescope's initial deployment in orbit on 24th April 1990. It was created from images taken by the Advanced Camera for Surveys Wide Field Channel (ACS/WFC). The dominant colours in the image were produced by gas ionised by ultraviolet radiation from the associated star cluster. The blue colour comes from glowing oxygen and the red colour from ionised hydrogen. The component images were acquired in November 2004.

Image courtesy NASA, ESA, and The Hubble Heritage Team (STScI/AURA)

HST News and Status

Jeremy Walsh

April 24th 2005 was the 15th Anniversary of the deployment into earth orbit of the Hubble Space Telescope. This milestone was celebrated in many ways and generated a huge amount of interest. One of the images released at this time is shown on the cover of this Newsletter, another appears on pages 6-7 and a DVD describing Hubble's technology and scientific achievements is enclosed. More details about the European celebrations are given in the article by Lars Lindberg Christensen on page 4.

Since the loss of the Space Telescope Imaging Spectrograph (STIS) in August 2004, the Hubble Space Telescope has settled down into routine operations. Indeed, the day-to-day functioning has been as smooth as ever, even to the point that guide star acquisition problems are now a rare occurrence. But of course Hubble is a mature telescope, and faces the universal problem of aging. With the requirement for three gyros and only four working, the life expectancy for astronomical observations is only a year or two. Since these parts are rather unpredictable in their failure rate, extrapolations are very uncertain. Hence the decision to implement a two-gyro mode, independent of whether there is to be a manned servicing mission to Hubble.

After over a year of preparation and simulations, the two-gyro mode software was uplinked to the observatory and tested in late February 2005. Expectations were high following the simulations, which had showed that typical jitter of around 10-12 milli-arcseconds could be expected. The tests went extremely well, with just a few missed guide stars leading to some failed observations. The aim of the tests was to measure the jitter for various observations with the ACS, NICMOS and WFPC2 instruments in a variety of situations. In addition there were engineering tests of the new pointing control system and the required modifications to scheduling procedures were exercised.

The assessment of the two-gyro science data indicates that the simulations, if anything, were somewhat pessimistic with respect to image quality. The tests indicate two-gyro image sharpness as good as in three-gyro mode. This means that, for instruments with larger pixels (NICMOS Camera 3, ACS/WFC and WFPC2), no degradation in the observed Point Spread Functions will be detectable at all. This achievement has been justly acclaimed and is a credit to the two-gyro science team from Goddard Space Flight Center. The most important impacts of switching to two-gyro observing will then be the reduction in the visibility of a given target through the year and additional overheads in the acquisition of targets. It has been decided to switch to two-gyro operation from the beginning of Cycle 14, due to begin around August 2005. Now that two-gyro mode has been shown to work, there are even rumours of a one-gyro mode. If the batteries last (deemed to be the next critical item in the failure path), then Hubble could even continue observing until the end of this decade without a servicing mission.

The HST Time Allocation meeting was held in late March 2005. The number of submitted proposals for Cycle 14 was down 24% on Cycle 13 and the number of requested orbits down by 18%, reflecting the loss of STIS, which in Cycle 13 was allocated 30% of orbits. The number of proposals with a European Principal Investigator (PI) was at the 15% level, slightly down on the fraction in previous cycles. The results were announced in early April and proposals with a European PI fared well in a typical culture of 4-5 times oversubscription for orbits. European PI proposals gained 18% by orbit and 26% by number of successful proposals. The latter figure is among the best ever results.

The new NASA administrator Mike Griffin appears to be taking a more open attitude to a manned servicing mission to Hubble, although a robotic servicing mission will no longer be considered. After the successful return to flight of the Shuttle fleet, imminent at the time of writing, a decision may be made to plan a servicing mission. This would then probably take place in 2008. During the mission the two instruments waiting on the ground – the Cosmic Origins Spectrograph (COS) and the Wide Field Camera 3 (WFC3) – would be installed, leading to a renewal in Hubble science from high resolution UV spectroscopy and deep UV and near-infrared imaging. After a year of pessimism about Hubble's future, this news is very encouraging.

ST-ECF Update

Bob Fosbury & Rudolph Albrecht

During the past two years, the ESA and ESO executives have been planning a long term role for the ST-ECF after the ESA part of the HST project winds down, whenever that may occur. Given their common interests in astronomy and the very large overlap between the communities they serve, both organisations have expressed a desire to maintain a joint ESA/ESO activity based at the ESO Headquarters in Garching. This group will carry out a range of technical, outreach and coordination tasks of interest and benefit to both parties.

Plans for the range of tasks assigned to the new group, and the staff necessary to carry them out, are currently being presented to the ESO and ESA advisory committees. Bob Fosbury assumed the leadership of the ST-ECF on June 1st 2005 and will be responsible for establishing a structure that will continue the HST activities and commitments as long as is necessary and be ready to take over the new tasks as required. Rudi Albrecht, who has been acting head of the ST-ECF for the last 21 months, will assist in this effort; he will also be spending part of his time working on behalf of ESA with the newly-formed European Space Policy Institute.

These new ESA/ESO tasks will be centered around high quality science data products and instrument calibration, the supply of compatible products to and the development of components for the Virtual Observatory – in collaboration with ESO and ESAC (VILSPA) – and the creation of public outreach material. In addition, the staff will be called upon to carry out ESO-ESA coordination tasks as required by the organisations.

Symphony of colours in the Tarantula

The Tarantula Nebula is the most vigorous star forming region known in the local Universe. Using the power of the freely available ESA/ESO/NASA Photoshop FITS Liberator package (http://www.spacetelescope.org/projects/fits_liberator) a young amateur astronomer has created this amazing panorama of the centre of the Tarantula. The original images were taken by the NASA/ESA Hubble Space Telescope and subsequently retrieved from the ESO/ST-ECF Science Archive in Munich, Germany.

Image courtesy: ESA/NASA, ESO and Danny LaCrue

The Tarantula Nebula, also known as 30 Doradus, is situated 170,000 light-years away in the Large Magellanic Cloud (LMC) in the Southern sky and is clearly visible to the naked eye as a large milky patch. Astronomers believe that this smallish, irregular galaxy is currently going through a violent period in its life cycle. It is orbiting the Milky Way and has had several close encounters with it. It is believed that the interaction with the Milky Way has caused an episode of energetic star formation – part of which is visible as the Tarantula Nebula. The Tarantula is the largest stellar nursery we know in the local Universe. In fact if this enormous complex of stars, gas and dust were at the distance of the Orion Nebula it would be visible during the day and cover a quarter of the sky.

Over the years the NASA/ESA Hubble Space Telescope has returned again and again to observe this interesting region of the sky and in this way Hubble has built up an archival treasure trove of more than a thousand images and spectra of the Tarantula. The 23 year old amateur astronomer Danny LaCrue sifted through the data and found that 15 of the exposures made with Hubble's Wide Field and Planetary Camera 2 could be combined to create a beautiful mosaic of the central parts of the unique Tarantula. Danny submitted his image to the Hubble European Space Agency Information Centre so that the image could be shared with a wider audience.

Hubble's 15th Anniversary – Facts about the ESA project

Lars Lindberg Christensen

April 24th 2005 marked the 15th anniversary of the launch of the NASA/ESA Hubble Space Telescope. As an observatory in space, Hubble is a major project that has made an enormous impact both in terms of scientific output and in its immediate public appeal.

Hubble has exploited its unique scientific capabilities in regions where no other instruments can compete. The telescope consistently delivers super-sharp images and clean, uncontaminated spectra over the entire near-infrared to ultraviolet regions of the electromagnetic spectrum. This has opened up new scientific territory and has resulted in many paradigm-breaking discoveries.

Exquisite quality images have enabled astronomers to gain entirely new insights into the workings of a huge range of different astronomical objects. Hubble has provided a visual overview of the underlying astrophysical processes taking place in these objects, ranging from planets in our Solar System to galaxies in the young Universe.

The renowned British astronomer Malcolm Longair writes in the preface to ESA's anniversary book: "*The Hubble Space Telescope has undoubtedly had a greater public impact than any other space astronomy mission ever. The images included in this beautiful volume are quite staggering in the detail they reveal about the Universe we live in and have already become part of our common scientific and cultural heritage.*"

The project

Many people agree that the long-term well-being and cultural development of European citizens depends on research and technological development. Information about science and scientists is a vital component of the scientific process, but the competition for attention in today's mass-media market is fierce. Attracting the attention of the younger generation with scientific information is especially difficult. Furthermore, in Europe, the cultural and linguistic diversity of the member states demands the development of multilingual products.

The 15th anniversary of Hubble's launch presented the ideal opportunity for a dramatic and dynamic project to grab the attention of the public, with a special emphasis on the younger generation, and to further the knowledge of science in general and astronomy in particular. In this project, Hubble was presented as a 'science superstar' to make the largest possible impact and reach as many different target groups as possible, including that section of the general population whose interest does not usually include science.

The project consisted of a number of activities, or vehicles to transport these messages:

- The full-length documentary movie "Hubble – 15 Years of Discovery" issued on DVD and for broadcast TV
- Events, planetarium shows and press meetings
- Educational Material
- Full-colour 120 page anniversary coffee-table book
- Movie Poster
- Movie soundtrack
- Planetarium Show Package for planetarium show production

More details about the individual activities are on the Anniversary web page: http://www.spacetelescope.org/projects/anniversary/

The movie covers all aspects of the Hubble Space Telescope project – a journey through the history, the troubled early life and the ultimate scientific successes of Hubble. More than half a million copies of the DVD have been distributed, making it possibly the most widely available science documentary ever.

The movie is presented by Bob Fosbury, head of the ST-ECF and a frequent user of Hubble for his own science. Through the movie Bob explains various astronomical phenomena and describes the workings of a major telescope like Hubble. As an active, but approachable scientist himself, we hope that Bob brings an added depth and insight to the material while simultaneously helping to demystify the image of scientists. Bob can perhaps serve as a role model for the younger generation and thereby help to 'dust off' this career choice. More about the movie on the back cover of this Newsletter.

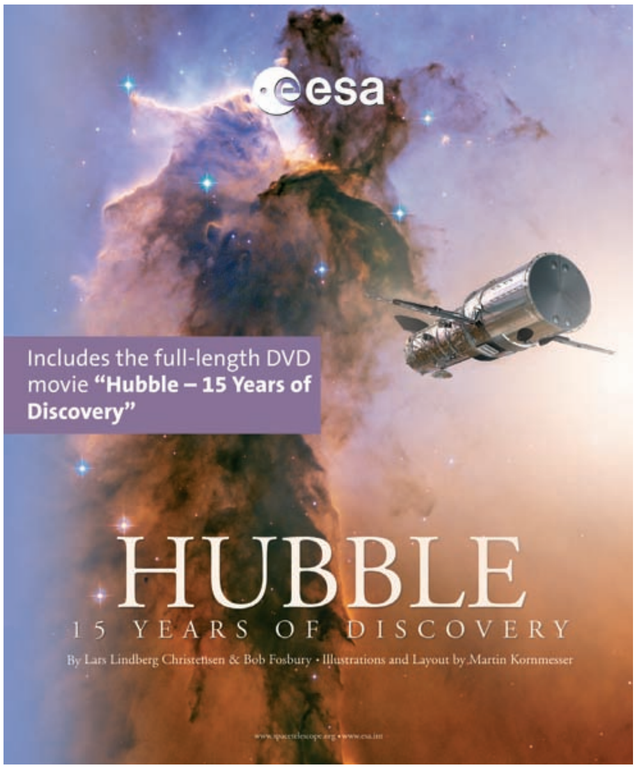

Cover of the ESA Hubble Anniversary Book. Astronomy is fortunate in that telescopes not only produce results of great scientific value, but also of eye-catching beauty and artistic potential. This book shows the close relationship between the two at its best. The book is 120 pages. 30 x 25 cm (coffee-table), full-colour, printed on high-quality glossy paper. It includes a copy of the DVD. Although 5,200 copies were made, all were distributed within a month. However, Springer in New York is printing a hardcover version of the book that will be distributed via Springer's normal channels. Translation to other languages is in progress.

Exploiting the trans-national dimension was seen as a natural and mandatory component of this project. Collaborators and partners from more than 20 EU member states and third countries joined in the collaboration. This truly unique multinational initiative created a multiple win-win situation for everyone involved from the participants in the production to the national partners and the end-users. Eventually a 'snowball' effect brought enough interested partners into the collaboration so that the production costs of the physical products such as DVD, book and exhibition panels were affordable for all involved. For example, some of the partners took out advertisements in large national newspapers and magazines for the DVD, thereby promoting Hubble and ESA in a way not otherwise possible, and so reaching target groups that we would normally not reach.

Hubble Day events

At more than 60 events all over Europe, Hubble's 15th anniversary was celebrated and the excitement of space shared: "Hubble Day", talks, the unveiling of two large, 3-metre anniversary images, exhibitions and more. Thousands of people heard talks by scientists and saw planetarium shows, images and movies of spectacular beauty. The close dialogue between public and working scientists was an integral part of the project.

Countries where events took place included:

Austria	Greece	Slovak Republic
Belgium	Hungary	Spain
Bulgaria	Italy	Sweden
Czech Republic	Lithuania	The Netherlands
Denmark	Poland	UK
France	Portugal	Ukraine
Germany		

Naturally, most of the EU member states are represented on this list, but it is worth noting the large enthusiasm with which other countries embraced this project and used it as an opportunity to further the interest in astronomy in towns and cities.

Credit: Nürnburg Planetarium.

One of the over 60 Hubble Day events in Europe, here Nürnburg Planetarium.

Logos of the 22 National Partners that were involved in the project collaboration.

Some numbers

- To match the individual cultures and national traditions 17 different DVD labels and 13 different cover versions were produced. Overall 22 different DVD 'packages' were made.
- 518,307 DVD copies of the first edition of the movie were distributed through more than 80 delivery points all over Europe (magazines, newspapers, science centres etc.). This makes it probably the most widely distributed science documentary ever.
- Around 20,000 DVD/CD Soundtrack bundles were sold inexpensively via the company SPV. This DVD/CD Soundtrack bundle even managed to make it into Amazon.de's top 100 CD Chart at number 83.
- An estimated 5-10 million viewers have watched the movie through various TV channels.

Conclusion

In many ways the European Hubble anniversary project can be seen as a role model for trans-national science communication and the informal network created here will be exploited for many years to come.

Acknowledgments

We would like again to thank everyone involved in this massive project! The list of people to thank is unfortunately too large for this article, but most are listed in the end-titles of the DVD. This project would never have happened without you!


News Release
heic0506
HUBBLE * EUROPEAN * SPACE AGENCY * INFORMATION * CENTRE

One of the two anniversary images (the other is featured on the Newsletter cover), the Whirlpool Galaxy (M 51) observed with the ACS on Hubble.
Credit: NASA, ESA, S. Beckwith (STScI), and The Hubble Heritage Team (STScI/AURA).

New Developments in aXe

Martin Kümmel, Søren Larsen & Jeremy Walsh

The aXe spectroscopic data extraction software was built for the reduction of large format slitless spectroscopic images. Its main application is the reduction of spectroscopic data taken with the Advanced Camera for Surveys (ACS) on Hubble, which offers slitless spectroscopy as an observing mode for all three channels.

aXe is distributed as part of the IRAF/STSDAS software package (subpackage 'hst_calib.acs.axe'). In addition to this the aXe webpages at http://www.stecf.org/software/aXe/index.html always offer the latest aXe release which can be installed and used as an external PyRAF package. The last major release, axe-1.4, was distributed in November 2004 within STSDAS 3.3 and is extensively described in the October 2004 ST-ECF Newsletter (see Kümmel et al. 2004).

In this article we present and describe new developments and features that are currently being implemented in aXe. Our main efforts concentrate on a more refined scheme to handle source contamination and the implementation of an optimal extraction algorithm (Horne, 1985) within aXe. The emphasis here is on the quantitative contamination.

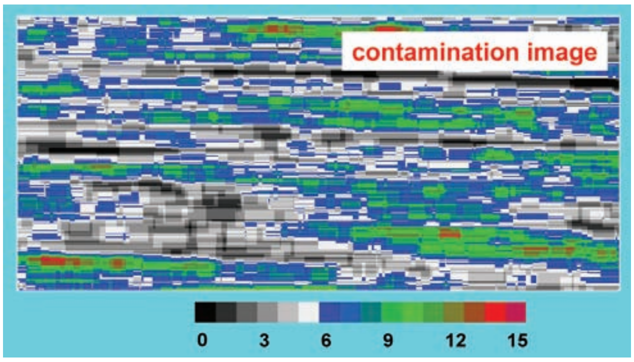

Fig 1: Contamination image compiled for data taken in the Hubble Ultra Deep Field. The different colours give the number of spectral orders which contaminate each other.

Contamination in Slitless Spectroscopy

In conventional spectroscopy the use of slits or masks prevents most of the light in the focal plane from entering the dispersing element. An overlay of spectra from different sources occurs only if two or more objects fall within the aperture defined by a slit or mask element. In slitless spectroscopy however, the lack of any spatial filtering of sources allows the overlap of spectra both from near neighbours in the cross dispersion direction and more distant sources in the dispersion direction. For this reason spectral overlap or contamination is an ubiquitous issue for slitless spectroscopy, which must be explicitly taken into account in the data reduction.

In aXe there is the possibility to record the areas covered by the different orders of all objects on a so called contamination image. Figure 1 shows the contamination image for data taken in the Hubble Ultra Deep Field (HUDF) (see Pirzkal et al. 2004). The black areas in Figure 1 mark regions covered by no spectrum at all, the red areas show regions which are covered by several (up to 15) overlapping spectra, which contaminate each other. The information on the number of contaminating sources in Figure 1 is fully propagated in the 1D extraction of the individual object spectra. As a final result each spectral element is accompanied by a flag which indicates whether its input pixels were also part of other object spectra. The regions of 1D spectra where the contamination flag is set must be used with care, since neighbouring sources also contribute to the extracted flux.

This contamination scheme is very efficient at identifying problematic regions in the individual object spectra, but it does not help the user to assess the severity of the contamination, and thereby decide whether the contaminated spectrum might still be suitable for further scientific analysis or not. While for faint objects the contamination from brighter sources is very severe and contaminated data points are usually unusable, for bright objects the contamination suffered from faint objects may affect the spectrum only marginally and, though the contamination flag is set, no restrictions need be applied to the data.

To solve this problem we have implemented in aXe a quantitative contamination scheme which gives, for each spectral element, an estimate of the contaminating flux from all other sources. Based on this quantitative contamination estimation the user has a better tool to decide which data points can be trusted. The aim here is not to provide decontaminated spectra, as that would require a deconvolution approach, but a reliable estimate of how a flux value can be trusted (effectively a systematic error).

Quantitative Contamination

The basis of the quantitative contamination estimation is a model which estimates the dispersed contribution of every object to the grism image. The contributions of the individual objects are then coadded into a 2D contamination image, which is a quantitative model of the examined grism image. In the 1D extraction of the individual object spectra, we subtract the model contribution of the object itself (to avoid self-contamination) and then process the data from the modelled grism image in parallel to the data from the real grism image.

As a result we derive two spectra for every object: one extracted from the real grism image and a second one extracted from the modelled grism image. Since the model contribution of the object itself was excluded in the extraction of the latter spectrum, this spectrum is a quantitative estimate of the contamination from all other sources to the object spectrum in question. The accuracy of the contamination spectrum is set by the accuracy of the input that is necessary to compute the modelled grism image.

For the modelling of the contribution of the different objects to the grism image, two different sets of input parameters are required:

- Description of the dispersing element: sensitivity, dispersion and location of the various grism orders

- An emission model: positions and morphologies; some spectral information of the emitting sources to disperse a coarse energy distribution to the resolution of the grism

For the description of the dispersing element we can use the sensitivities and parameters which are compiled and used for the spectral extraction from the grism images. For the emission model, there are several different ways to specify the various components. We have implemented two different emission models, called the *Gaussian Emission Model* and the *Fluxcube Model*.

The Gaussian Emission Model

In the Gaussian emission model the object morphologies are approximated by Gaussians with widths taken from the input direct image catalogue. The spectral information is given by the total AB-magnitude in at least one filter passband or one wavelength.

All necessary object information is specified in various columns of the Input Object List, an ASCII table with a format similar to the SExtractor output tables (see the aXe manual for details). In fact, the basic Input Object List that is required to run aXe contains all the data to compute the contamination with the Gaussian emission model.

Figure 2 displays on the left side the direct images of the Gaussian emission model in four filters for data taken in the HUDF. The right side of Figure 2 shows the modelled grism image computed

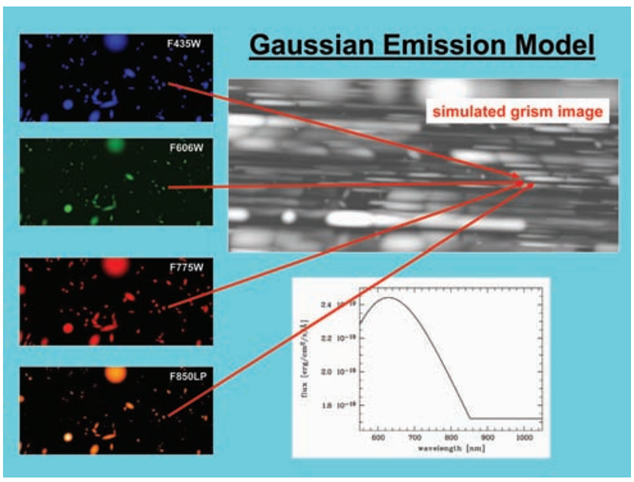

Fig 2: Gaussian emission model: spectral information in four filters (left) is employed to compute the model grism image (right). The arrows connect the direct image positions of one object to its first order grism spectrum. The full spectrum used to model this object is also displayed (lower right).

from the spectrum with the Gaussian emission model. The arrows point from the direct image positions of one object to the position of its first order spectrum in the modelled grism image. The spectrum which was employed to model this object is plotted in the lower part of Fig. 2. The interpolated data in between the data points derived from the AB-magnitudes (at 435, 606, 775 and 850 nm) are computed with a cubic spline, outside of the data points the spectrum is a constant extrapolation of the last data point.

The images in Figure 2 cover the same area as the contamination image in Figure 1. The direct images in Figure 2 were only created for illustration purposes. In real aXe runs, each filter is just represented by a column in the Input Object List which gives the total AB-magnitude of the objects.

The Fluxcube Model

In the Fluxcube emission model both the object morphologies and the spectral information are taken from the fluxcube file associated with every grism image. A fluxcube file is a multi-dimensional FITS image with one or several flux images taken at different wavelengths as extensions. The basis of the flux images are normal 2D images in [counts/sec], which must be transformed to flux in [erg/cm^2/s/Å] using the appropriate zeropoints. All extensions of the fluxcube image must cover the same area as the corresponding grism image.

The flux extensions in the fluxcube provide sufficient information to compute a model grism image. In the determination of the quantitative contamination however, it is essential to derive the individual contribution of each object to the modelled grism image. This addition is necessary to be able to subtract the self contamination and to isolate the contamination from other sources for each individual object.

For this reason the first extension of a fluxcube image must contain a so called "segmentation image". In the segmentation image each pixel value is the (integer) number of the object to which the pixel is attributed. The SExtractor software (see Bertin & Arnouts 1996) provides the possibility to create a segmentation image (parameter setting: "CHECKIMAGE_TYPE SEGMENTATION") as an additional output product of the source extraction.

The fluxcube files necessarily follow a rather complicated file format. To support the user in the creation of fluxcube files we have implemented a new aXe task. The new task works in a standard scenario with a MultiDrizzled grism image, one or several MultiDrizzled direct images and a segmentation image as input.

As an illustration of the fluxcube model, Figure 3 shows on the left side the segmentation image and the filter images used to create the fluxcube. The lower right part of Figure 3 displays the modelled grism image derived by the fluxcube emission model. All images in Figure 3 cover the identical area to Figures 1 and 2 in the HUDF.

Both emission models have advantages and disadvantages. The spectral information in the fluxcubes differs from pixel to pixel. This emission model provides an extremely detailed and accurate input for the computation of the quantitative contamination. But sufficiently deep multi-colour data may not always be available to exploit the capabilities of the model. The Gaussian emission model demands less sophisticated input and, moreover, in this model it is possible to take into account variations of the point spread function with wavelength. On the other hand, the Gaussian approximation of the object emission with identical spectral information over all its area is rather coarse.

The differences between the new quantitative contamination scheme and the old, 'geometrical' contamination is demonstrated in Figure 4. In the lower panel the red line indicates spectral elements with the (old) contamination flag set. All data longwards of 6200Å is suspected to be significantly influenced by contamination. The upper panel shows in black the spectrum extracted by aXe, and in red the sum of the spectral contribution of all contaminating sources according to the Gaussian emission model. It is immediately clear that, within the accuracy of the emission model, the contaminants' contribution to the object spectrum is negligible; there are thus no restrictions for the scientific use of the object spectrum.

Simulating Grism Images

A central item within the quantitative contamination scheme is the computation of the model grism image associated with the real grism image. Since all input to the quantitative contamination model is independent of the particular grism image for which the model is computed, the quantitative contamination can be used to create simulated grism images (eg, Figures 2 and 3). In order to perform the simulations, Input Object Lists of the region of interest can be compiled from archived Hubble or ground-based data. It is sufficient to use any archived grism image as a template image in the aXe reduction, ie, the observed region in the fake image can be completely disconnected from the region for which the simulation is made.

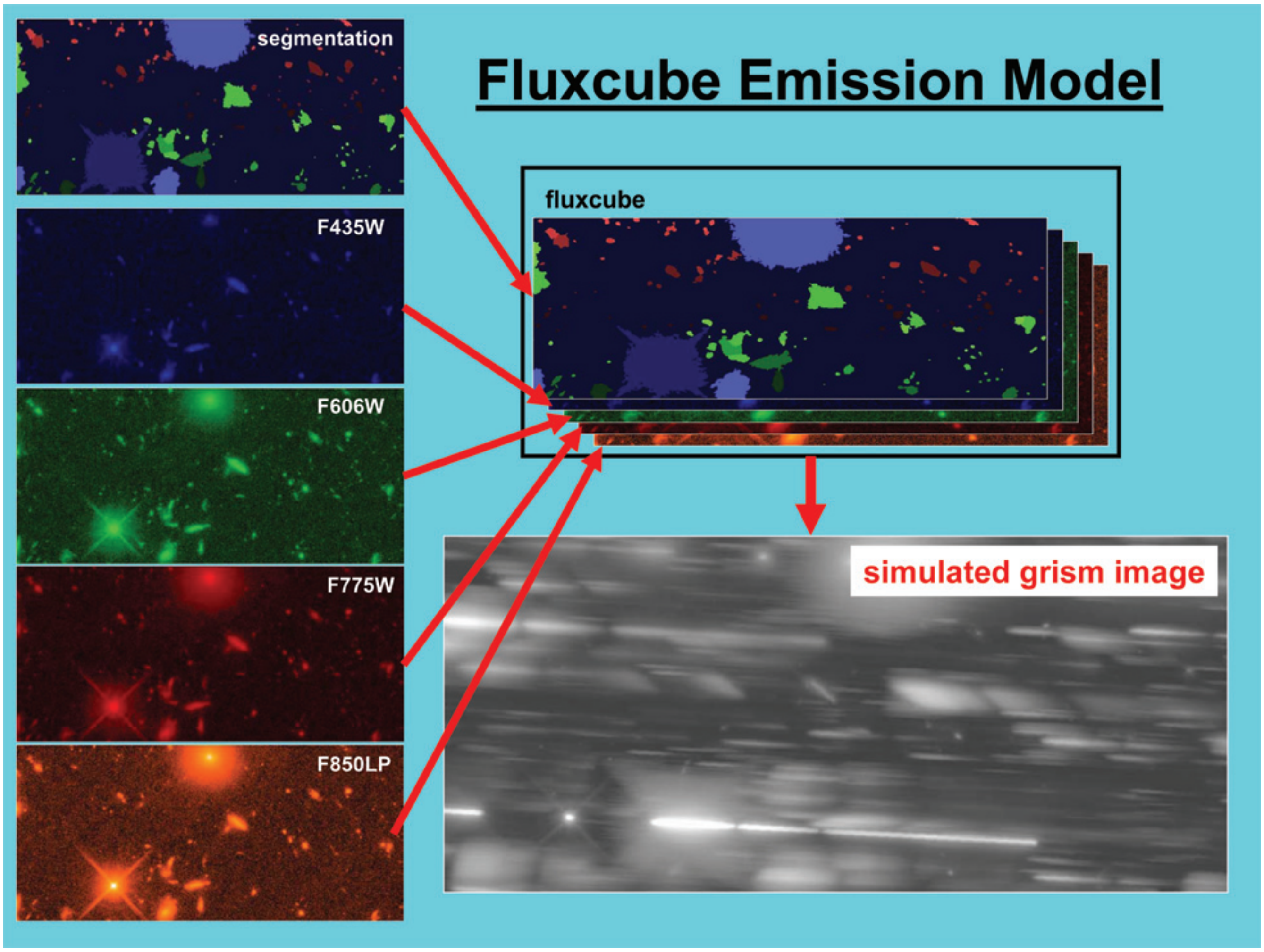

Fig 3: Fluxcube emission model: real images in four filters (left) are converted to flux images and combined with the segmentation image to create a fluxcube file (upper right). The model grism image (lower right) is computed using the data in the fluxcube.

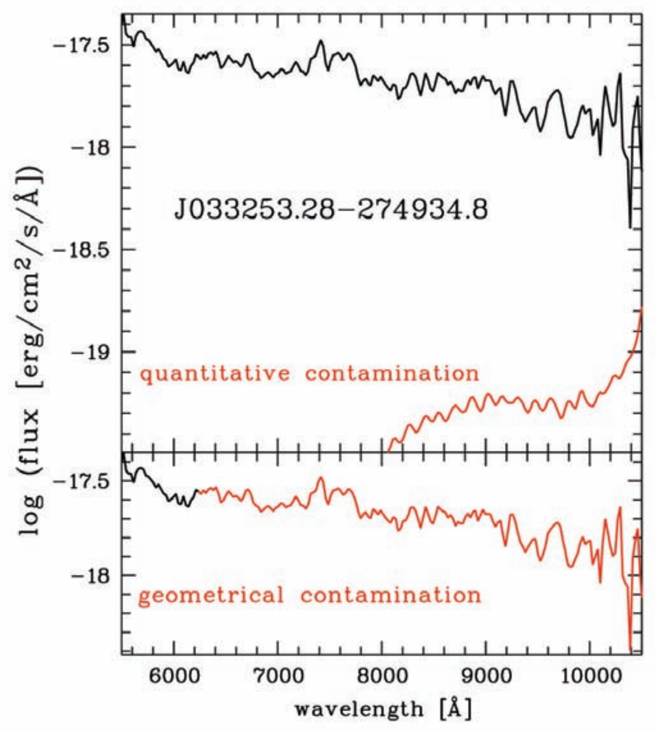

***Fig 4:** Extracted spectrum of an object and its contamination information. The old, 'geometrical' contamination scheme (lower panel) just marks suspicious spectral regions. The quantitative contamination (upper panel) gives an estimate of the contaminating flux from other sources.*

An important application of the capability to simulate grism images is the planning of grism observations with ACS. With the computation of several simulated grism images on the basis of a set of Input Object Lists with rotated image coordinates (using the Gaussian emission model), it is possible to investigate the optimum roll angle for an observation, such that surrounding objects, or the higher order beams from known objects outside of the field of view, do not contaminate the target object.

As a tool for observation planning, quantitative contamination complements rather than competes with the SLIM software package:
(http://www.stecf.org/software/SLIM/SLIM10/index.html) which was specifically designed for this purpose. SLIM creates the simulations on a completely general basis and uses standard spectra and instrumental throughput curves to place the object with the desired properties (eg, morphology, magnitude and redshift) on the grism image. The quantitative contamination, on the other hand, uses already observed object properties, stored as object lists with source sizes and magnitudes in different wavelengths, to simulate the grism images. An advantage of the quantitative contamination scheme is the usage of the configuration and sensitivity files which are also used for the source extraction. This guarantees the concordance of the simulated grism images with real data. Moreover, faster processing time allows the simulations of a much larger number of objects than in SLIM.

Towards aXe-1.5

The quantitative contamination will be a major addition to the next aXe-1.5 release which is projected for Autumn 2005.

Additional items to be included in aXe-1.5 are:

- **Optimum extraction**: We are currently investigating the various techniques for weighted extraction (eg, Horne 1986 or Robertson 1986) to isolate the best approach for slitless spectroscopic images.

- **Stellar extraction**: aXe-1.5 will include an extraction mode with a fixed extraction box and a fixed extraction direction perpendicular to the trace for all objects. This extraction mode will be particularly useful in cases of pointlike objects or for the faintest objects on the grism image. For those object classes, the morphology parameters measured in SExtractor (semimajor and semiminor axis and position angle of the semimajor axis), which are usually the basis of the aXe extraction width and extraction direction, can reflect the measurement errors rather than intrinsic object properties. Here the usage of fixed extraction quantities gives a clear advantage.

- **Early error detection**: Depending on the number of objects to be extracted the High Level aXe Tasks (introduced in aXe-1.4, see Kümmel et al. 2004) may have to run for several hours. If, in such a scenario, an error, eg, a missing sensitivity file, is discovered after some hours, the whole High Level Task must be repeated and the user has lost a large amount of computing time. To avoid such costly losses we have implemented an input control at the beginning of each High Level Task, in order to facilitate early error detection.

References

- *Horne, K. 1985, "An optimal extraction algorithm for CCD spectroscopy", PASP, 98, 609*
- *Kümmel, M., Walsh, J., Larsen, S. & Hook, R. 2004, "Drizzling and the aXe slitless spectra extraction software", ST-ECF Newsletter, 37, 14*
- *Pirzkal, N., Xu, C., Malhotra, S., Rhoads, J. E. et al. 2004,"GRAPES, Grism Spectroscopy of the Hubble Ultra Deep Field: Description and Data Reduction", ApJS, 154, 501*
- *Bertin, E. & Arnouts, S. 1996, "SExtractor: Software for source extraction", A&AS, 117, 393*
- *Robertson, J.G. 1986, "Optimal extraction of single-object spectra from observations with two-dimensional detectors", PASP, 98, 1220*

STIS Charge Transfer Inefficiency Correction Science Case: The Proper Motion of the Ursa Minor Dwarf Galaxy

Paul Bristow, Slawomir Piatek (New Jersey Institute of Technology) & Carlton Pryor (Rutgers)

The ST-ECF Calibration Enhancement effort for the Space Telescope Imaging Spectrograph (STIS) aims to improve data calibration by applying physical modelling techniques. As part of this effort, we have developed a model of the STIS CCD readout process that is able to correct STIS data for charge transfer inefficiency (CTI).

Without a model of the readout process, remedies for CTI have been limited to empirically derived adjustments to flux measurements for extracted stellar sources only. We have developed a detailed simulation of the readout process (Bristow & Alexov 2002, Bristow 2003b, Bristow 2004a), with which it is possible to correct the flux distribution in the image array. This approach has many benefits. It increases the accuracy of the flux correction and, more importantly, corrects the flux within extended objects. Thus, it restores the shape of a stellar image and so improves astrometry. The application of this simulation to the correction of data and early test results were discussed in an earlier issue of this newsletter (Bristow 2003a). The pipeline implementation of this technique is currently being evaluated at STScI.

This article discusses an example of the impact of the CTI correction upon a science project which requires the highest precision obtainable with Hubble, in this case astrometric precision. Piatek et al. (2002, 2003, and now 2005) report measurements of the proper motions of several nearby dwarf spheroidal galaxies. The required level of astrometric accuracy necessitates thorough data reduction, in particular the removal of any epoch-dependent effects.

CTI-Induced Centroid Shifts

Imperfect charge transfer results in some fraction of the charge contained in a charge packet being left behind as the packet is transferred across the chip. The larger amount of charge left behind by a large packet is likely to then join the subsequent, smaller, charge packets (eg, Janesick 2001). This redistribution of charge, ie, flux, has several consequences. Most directly, the peak intensity of a source decreases. Even the measured total flux decreases as flux is redistributed outside of the measurement aperture. The source morphology changes such that the centroid shifts in the direction away from the readout register. The effects upon morphology and centroid are relatively small, but are significant for astrometry needing the highest possible precision, such as the motions of nearby galaxies.

Analysis of CTI-affected data has revealed that the flux loss from sources is a function of position on the chip (distance from the readout register), background, signal strength, and epoch (eg, Kimble et al. 2000). These dependencies can be understood by considering a population of charge traps on the detector that are produced by radiation damage. The dependence on epoch reflects the increase in radiation damage with time in orbit. The dependence on source strength arises from a larger charge packet having a greater cross-sectional area and, therefore, encountering more traps. Higher background signals fill traps, leaving fewer empty traps to be filled by signal from a source. Finally, a greater distance from the readout register implies more transfers and more chances for trapping. All of these are reflected in the empirical corrections available for CTI (Goudfrooij & Kimble 2002, Dolphin 2002) and are reproduced by our readout model (Bristow 2003b).

The size of the centroid shift has not been as precisely parameterised as has been the size of the flux lost, but it will depend upon the same factors. Figure 1 is a schematic illustration of the CTI-induced shift in an image centroid, Δy. The black profile is the distribution of charge from a point source along the parallel readout direction for CTI-free data. The red profile is the distribution that would be measured in the presence of CTI. The figure shows that the centroid shifts are always in the same direction: aligned with the parallel readout axis and away from the readout register. This ignores the serial CTI effect which contributes a component along the serial axis, but is at least two orders of magnitude smaller. Since the readout register is at the top of a STIS image, the centroids of sources in these images shift downwards. The size of the shift should increase with increasing distance from the readout register and also depend on both the flux of the individual source and the background signal level in the image. The shifts should be larger in more recent datasets because of the larger amount of radiation damage.

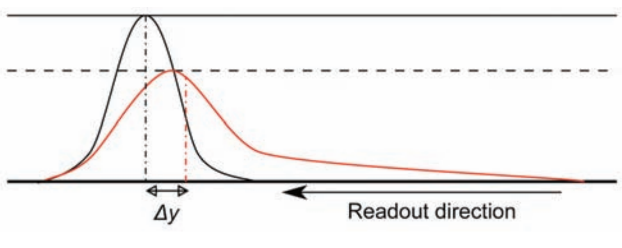

Fig 1: *Distribution of charge from a point source along the parallel readout direction without (black) and with (red) CTI.*

Proper Motions of Dwarf Spheroidal Galaxies

Piatek et al. (2002) and Piatek et al. (2003) detected and measured the motions of dwarf spheroidal galaxies in the neighbourhood of the Milky Way Galaxy using STIS CCD imaging data and WFPC2 PC data. They compared the relative positions of constituent stars to a background QSO at three epochs separated by several years. For Fornax, the measurements from three fields produced consistent estimates for the proper motion. For Carina, measurements from two fields also agreed. Piatek et al. (2002, 2003) used the measured proper motions to derive the orbital parameters of these two galaxies.

The accuracy of the astrometry required to make such measurements is barely achievable even with cameras on Hubble. Exactly this kind of measurement may be sensitive to the very small and time-dependent systematic offset of centroids introduced by CTI. The analysis of Piatek et al. employs dithered exposures to better sample the PSF, makes a rigorous determination of the effective PSF, enforces strict selection criteria for the stars considered, and takes proper account of such effects as geometric distortion.

At the time of these studies, there was no method available for correcting the shifts in the positions of stars and the QSO caused by CTI. Bristow (2004c) identified these measurements as potentially sensitive to CTI effects and used the aforementioned readout simulation to estimate the size of CTI effects in the data. This preliminary estimate revealed that the different size of the CTI-induced shifts for specific datasets from two separate epochs *could* change the measured proper motions of individual stars significantly.

The measured proper motion of a dwarf spheroidal galaxy derives from the shift in the bright QSO relative to the mostly fainter member stars, so a precise estimate of the impact of CTI must include the dependence on flux in multiple datasets with different orientations and different background levels. Bristow (2004c) also noted that the Piatek et al. analysis could be affected in subtler ways. For example, their adoption of a uniform PSF across the image array, driven by the scarcity of stars in the field, is more likely to lead to errors in the presence of position-dependent CTI effects.

Therefore, the best way to remove CTI effects from such proper motion measurements is to use as input data which have been corrected with the computer code described by Bristow (2004a, 2003b) and Bristow & Alexov (2002).

The Ursa Minor Dwarf Galaxy

Piatek et al. (2005, hereafter P05) present a measurement of the proper motion of the Ursa Minor dwarf spheroidal galaxy using data from two distinct fields, one imaged with the STIS CCD and the other with the WFPC2 planetary camera. In this study, the data taken with STIS were restored with the CTI correction code before being analysed using the same procedure as that for Fornax and Carina.

The STIS data come from three epochs: February 2000, February 2001 and February 2002. The first two epochs consist of 8 observations each with 6 dithered sub-exposures and the last epoch also has 8 observations but with 3 dithered exposures. All of the 120 raw exposures were corrected for CTI and then processed by the CALSTIS pipeline up to and including flat fielding. Header switches took their nominal archive values except for DARKFILE. The standard dark reference file for each dataset was itself corrected with the CTI code and the corrected dark file was then used in the reduction of the dataset (as described in Bristow 2004b). The details of the subsequent analysis are given in P05.

Figures 2a and 2b show a 296 x 259 pixel section, centred at pixel location 184,262 (RA $15^h08^m36.636^s$, Dec +67°16'54.18'') of one of the 3rd-epoch raw datasets (O6D901010) without and with CTI correction, respectively. The charge trails below objects in Figure 2a – the readout direction is up in this image – show the impact of the CTI and they are reduced or removed in the corrected data.

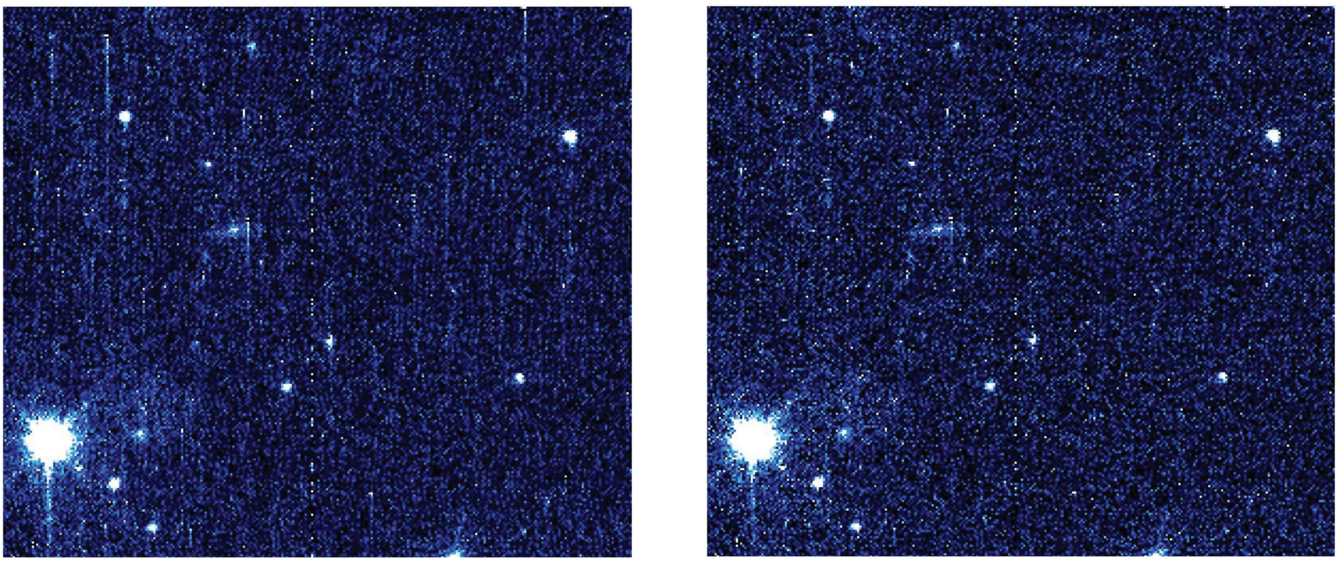

Fig 2: *A section of an image from the third epoch data a) without CTI correction and b) with CTI correction.*

Figure 3 shows the difference between the Y coordinates of the centroid measured from corrected and uncorrected data, Δy, as a function of row number. Because the Y axis is the parallel readout direction, Δy is the shift caused by CTI. Note that the shift is largest for small row numbers because these pixels are farthest from the readout register. The crosses are for all 8 datasets at the first epoch and the squares are for the data at the third epoch. The selection criteria here are the same as described in Piatek et al. (2003) and used in P05.

Figure 3 shows that the average Δy is greater and Δy increases more rapidly with distance from the readout register at the later epoch than at the earlier one. This is as expected due to the increased radiation damage at the later epoch. The dashed and solid lines are linear fits to the points from the earlier and later epochs, respectively. A measure of the average difference in Δy between epochs at a given row number is the vertical distance between the two lines. The average difference for all of the stars is this vertical distance at the centre of the frame.

The green circles highlight the shifts for the QSO at each epoch. The QSO has a relatively small CTI-induced shift at each epoch. Even more importantly, the difference between the shifts for the two epochs is very small for the QSO, smaller than the average difference between the Δy values for the stars. In addition, note that the positions of the QSO and all of the stars are about 50 pixels farther from the serial register in the readout (y) direction at the later epoch. Thus, all of the stars common to the two epochs have an additional about 150 extra charge transfers (50 pixels x 3 clock phases) at the later epoch and, for this reason, the difference in the average Δy between the two epochs is the vertical distance described above plus the increase in Δy given by the slope of the solid line times about 50 pixels.

The overall CTI-induced shift is smaller for many stars in these data than the scatter in the Δy values from different datasets within an epoch. The red squares in Figure 3 highlight the data from all 8 datasets for one star at the later epoch. The scatter is large, but there are several reasons for it which all derive from the fact that the model correcting the CTI takes into account the status of charge traps during the readout. For example, a cosmic ray between the source and the serial register can reduce the effect of CTI on that source in that particular exposure because the traps are more likely to be full as the source charge packets are read out. Another factor is the column in which the source is located – a dither may move the source into a column with a different distribution of hot pixels between the source and the serial register. Also, the dark frame itself is corrected for CTI and the dark signature will be aligned differently with respect to the sources for different dither positions. A smaller effect is that sub-pixel dithers cause the flux profile along a given column to change shape slightly, causing a small change in the capture of electrons in the readout. Finally, Poisson noise in pixel values differs between exposures, causing a significant random effect in the filling of traps – the trap array status at any instant during the readout can be said to have its own noise component. In other words, a noise spike immediately before a source in the readout direction can change the amount of charge that would be trapped from the source.

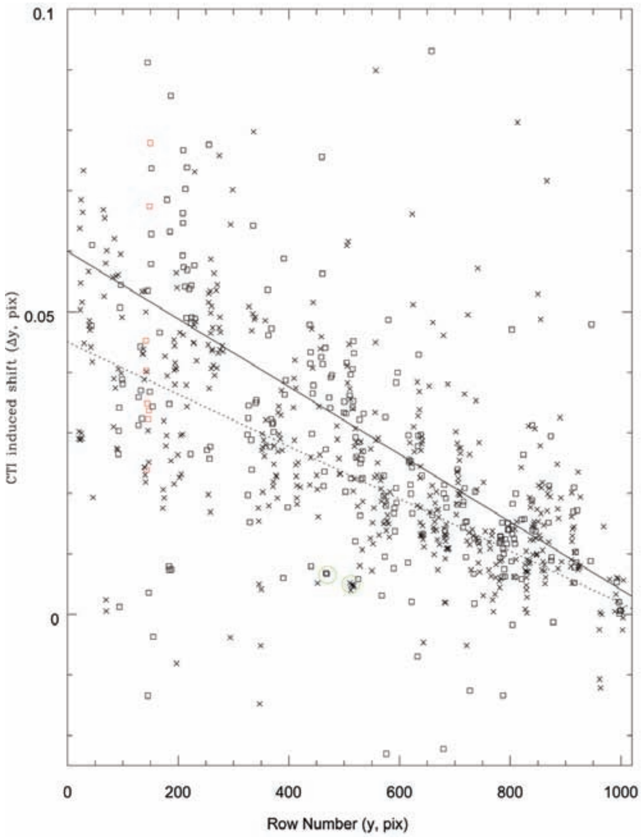

Fig 3: *CTI-induced shift (Δy) versus row number (small row number being farthest from the serial register) for all eight datasets in the 2000 epoch data (crosses) and the 2002 epoch data (squares). The green circles highlight points corresponding to the QSO. The red squares are the points for one star in the 2002 epoch data.*

Figure 4 shows how correcting for CTI ultimately affects the proper motion derived for Ursa Minor. The proper motion estimates obtained by applying the analysis of P05 to CTI-corrected and CTI-uncorrected data are plotted. The impact is significant compared to the uncertainties, which represent the estimated errors from sources other than CTI. Encouragingly, the proper motion estimated from CTI-corrected STIS data is in better agreement with the result from the field imaged with WFPC2.

WFPC2

Since the CTI effects seen in the STIS data are important, we expect that the WFPC2 PC data have the same problem. WFPC2 has, after all, been on orbit three years longer and is known to have more serious CTI than STIS, ameliorated slightly by the smaller chip size. Unfortunately, adapting our CTI code for WFPC2, though desirable for many reasons beyond just this project, is not a trivial undertaking. Instead, P05 compute an empirical correction to the centroids derived from WFPC2 PC data as a linear function of distance from the serial register. The empirical fit is specific to each epoch and is based upon a larger data

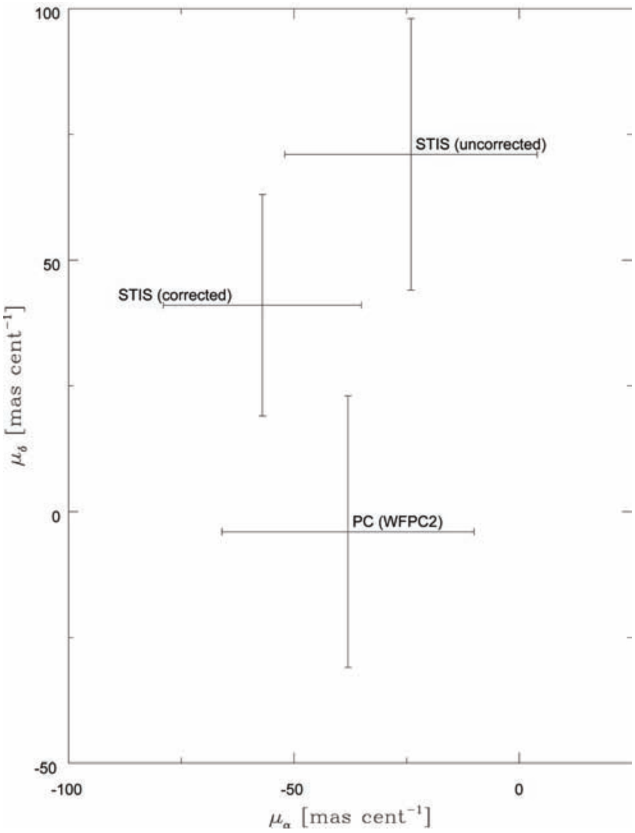

Fig 4: *Measurements of the proper motion for Ursa Minor after application of the full analysis of Piatek et al. (P05).*

set collected as part of the same project but for the Fornax dwarf spheroidal galaxy. To our knowledge, this is the first time that a CTI-induced centroid shift has been calibrated in this way.

Further Applications

Similar proper motion measurements are in progress for Sculptor and Fornax, the latter using a longer time baseline than that used by Piatek et al. 2002. The data for these studies have already had the CTI correction applied. The results of the full analysis will appear in future publications.

References

- *Bristow, P. 2003, ST-ECF Newsletter, 34, 9 (2003a)*
- *Bristow, P. & Alexov, A. 2002, ST-ECF Instrument Science Report, CE-STIS-ISR 2002-001*
- *Bristow, P. 2003, ST-ECF Instrument Science Report CE-STIS-ISR 2003-001 (2003b)*
- *Bristow, P. 2004, ST-ECF Instrument Science Report CE-STIS-ISR 2004-001 (2004a)*
- *Bristow, P. 2004, ST-ECF Instrument Science Report CE-STIS-ISR 2004-002 (2004b)*
- *Bristow, P. 2004, ST-ECF Instrument Science Report CE-STIS-ISR 2004-003 (2004c)*
- *Cawley, L., Goudfrooij, P. & Whitmore, B. 2001, STScI Instrument Science Report WFC3 2001-05*
- *Dolphin, A. E. 2002, in "Proceedings of the 2002 HST Calibration Workshop", Eds Arribas, S., Koekemoer, A and Whitmore, B., Space Telescope Science Institute, 301*
- *Goudfrooij, P. & Kimble, R. A. 2002, in "Proceedings of the 2002 HST Calibration Workshop", Eds Arribas, S., Koekemoer, A and Whitmore, B. Space Telescope Science Institute, 105*
- *Heyer, I. 2001, STScI Instrument Science Report WFPC2 2001-009*
- *Janesick, J. 2001, Scientific Charge Coupled Devices, SPIE, ISBN 0-8194-3698-4, 387*
- *Kimble, R. A., Goudfrooij, P. & Gilliland, R.L. 2000, in Proc. SPIE "UV, Optical, and IR Space Telescopes and Instruments", James B. Breckinridge; Peter Jakobsen; Eds., 4013, 532*
- *Piatek, S., et al. 2002, AJ, 124, 3198*
- *Piatek, S., et al. 2003, AJ, 126, 2346*
- *Piatek, S., et al. 2005, AJ, 130, 95 (P05)*

Supernova remnant menagerie

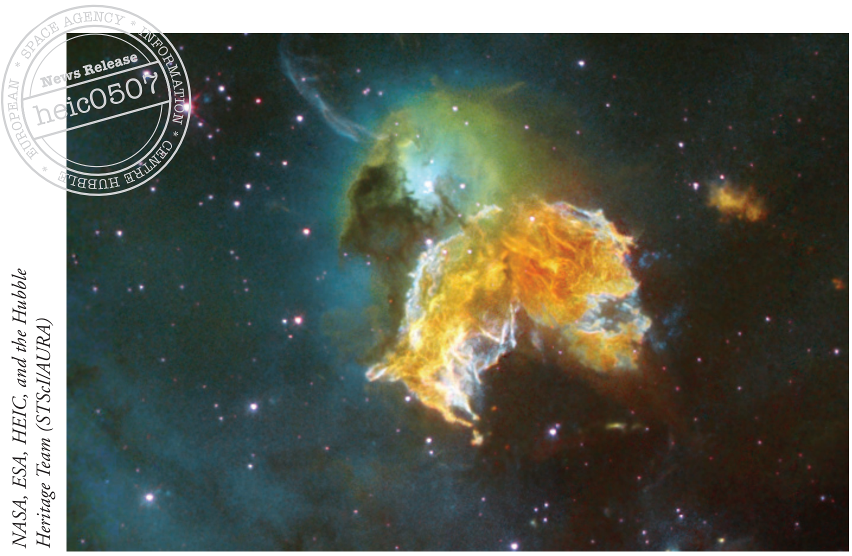

NASA, ESA, HEIC, and the Hubble Heritage Team (STScI/AURA)

A violent and chaotic-looking mass of gas and dust is seen in this Hubble Space Telescope image of a nearby supernova remnant. Denoted N 63A, the object is the remains of a massive star that exploded, spewing its gaseous layers out into an already turbulent region.

The supernova remnant N 63A is a member of N 63, a star-forming region in the Large Magellanic Cloud (LMC). Visible from the southern hemisphere, the LMC is an irregular galaxy lying 160,000 light-years from our own Milky Way galaxy. The LMC provides excellent examples of active star formation and supernova remnants, many of which have been studied with Hubble.

MultiDrizzle in the Hubble Archive Pipelines: Automatically Cleaned, Combined Images

Anton M. Koekemoer (STScI)

Observations obtained with Hubble are often divided into multiple separate exposures, in order to be able to remove a variety of artefacts that are generally present in the images. These artefacts include random cosmic rays striking the detectors, as well as bad pixels and other defects that are inherent in the detectors themselves. Dividing the observation into separate exposures allows the cosmic rays to be removed during processing, since they are different in each exposure. In addition, if the separate exposures are shifted to slightly different positions on the sky, or "dithered", then detector defects can also be removed, since they are moved to different locations on the sky relative to the astronomical objects. Another advantage of dithering is that it can be used to improve the spatial resolution and sampling of the data, since the Hubble point-spread function (PSF) is generally undersampled by the detector pixels. Obtaining subpixel shifts allows a sharper image to be produced when the exposures are combined using software such as "Drizzle" (Fruchter & Hook 2002), which improves sampling and optimizes spatial resolution while maintaining photometric and astrometric fidelity.

The subsequent development of MultiDrizzle (Koekemoer et al. 2002) has provided an automated means of registering images, removing cosmic rays, bad pixels and other detector artefacts, and using "Drizzle" to combine the images and remove the geometric distortion. MultiDrizzle thus replaces a series of complex and labour-intensive tasks with a seamless, integrated tool to clean and combine images. For data that are optimally dithered, this produces an output image that is clean from cosmic rays and other significant defects, while at the same time improving the sampling and resolution, and the photometric and astrometric quality of the data.

In September 2004, MultiDrizzle was incorporated into the Hubble Archive Pipeline at STScI, providing for the first time fully automated cleaning and image combination of all associated sequences of dithered exposures obtained with the Advanced Camera for Surveys (ACS). Prior to this, requests for associated exposures from the science archives produced limited cosmic ray cleaning, only in cases where dithering had not been used. Subsequently MultiDrizzle was also made available for users of the Hubble archives at ST-ECF and CADC using the same core software. The inclusion of MultiDrizzle now results in the delivery of a clean, combined image for any associated set of ACS exposures that is requested from any of the three Hubble archive pipeline sites. MultiDrizzle is run on images that have passed through the essential steps of calibration, which include bias subtraction, flat fielding, and dark current correction.

Given a set of input exposures, MultiDrizzle carries out the following steps in sequence:

- Calculate and subtract a background sky value for each exposure;
- Search for additional bad pixels in each exposure, that are occasionally not flagged during calibration;
- Determine shifts from the coordinates in the image headers, and apply these shifts in drizzling all the exposures onto a series of separate output images that are registered on a common grid;
- Use the drizzled exposures to create a first-pass cleaned image, which is essentially a sigma-clipped median image;
- Transform the first-pass clean median image back to the frame of each original input exposure;
- Compare each input exposure with the clean image to create a cosmic ray mask;
- Use Drizzle to combine all the input exposures, weighted by their cosmic ray masks, thereby creating a final cleaned output image.

The parameters for MultiDrizzle have been set so that the combined image products from the Hubble archive pipelines should be scientifically useful in the majority of cases, without the need for further processing by observers. The initial implementation of MultiDrizzle in the Hubble archive pipelines for the ACS/WFC, HRC and SBC cameras can generally be expected to provide useful images for datasets where the standard recommendations of dithering were followed. This includes obtaining at least four images of comparable exposure time, together with the use of a dither pattern or CR-SPLIT to ensure that the exposures are properly associated within the pipeline systems. If observers request the calibrated output products for ACS associations, then they automatically receive the cleaned MultiDrizzle output image along with all the separate exposures and other related files.

An example of the type of output produced by MultiDrizzle is shown in Figure 1, where MultiDrizzle was run with all its default parameters on a 4-exposure dithered observation of the galaxy NGC 4594. The image demonstrates the good quality of the automated cosmic ray removal within MultiDrizzle, along with the accuracy of the registration obtained from the image headers.

The MultiDrizzle software is also made available for observers to run off-line with their own parameters, in case this is required to optimize the images for some scientific applications. For example, observers may wish to use a finer pixel scale, or a different orientation. This can be easily achieved by running MultiDrizzle within the observers' own IRAF/STSDAS environment once the data have been retrieved.

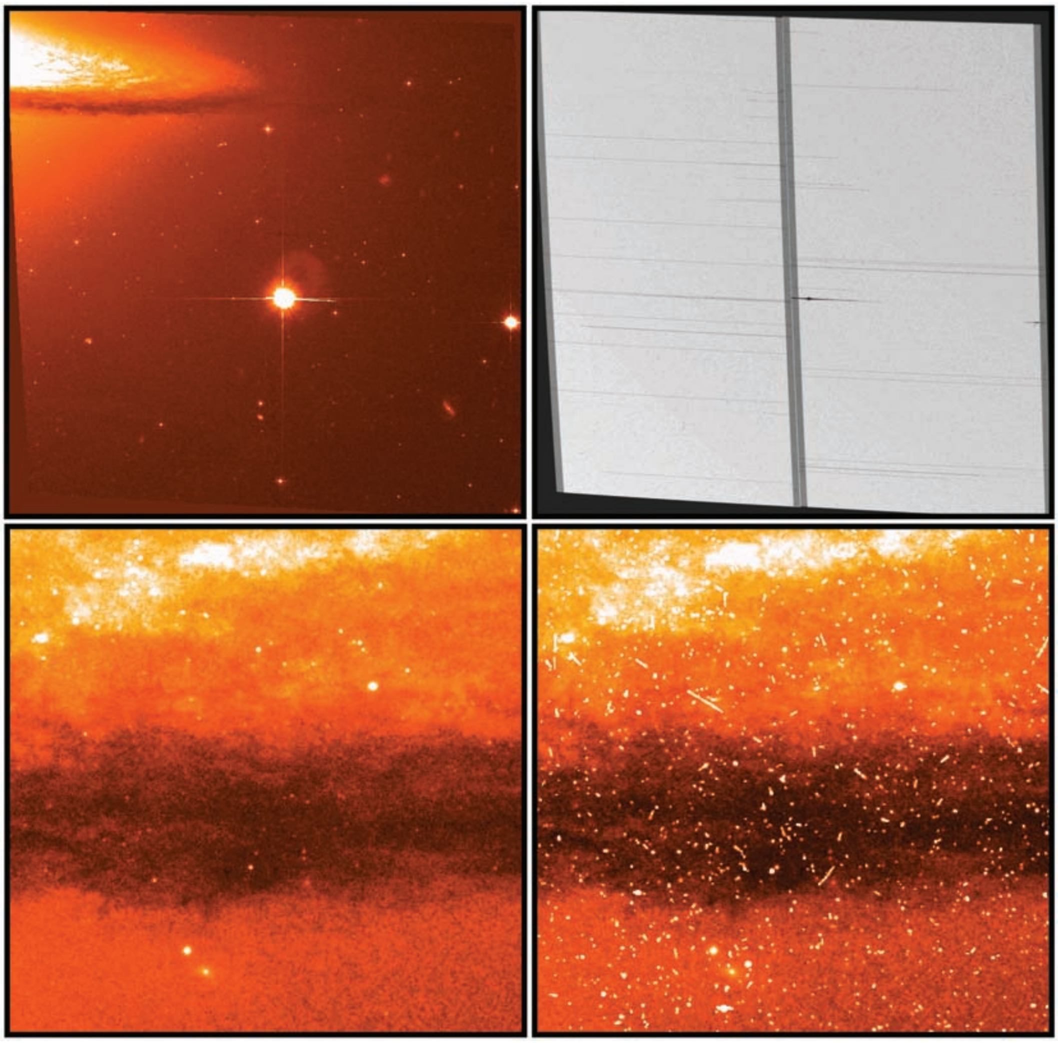

Fig 1: Example of the automatically cleaned MultiDrizzle product, for a 4-exposure dithered observation of the nearby galaxy NGC 4594. The top panels show the final full-frame drizzled and weight images (left and right, respectively). The bottom left panel shows a close-up of the output image from MultiDrizzle, while the bottom right panel shows the sum of all the accumulated cosmic rays originally present in the exposures.

We are continuing efforts to generalize MultiDrizzle to other Hubble instruments, as well as adding new capabilities to it. The off-line version available within IRAF/STSDAS is tested for both ACS and WFPC2 data, and some support is also available for NICMOS and STIS imaging data. Other enhancements, for example the ability to empirically refine the header-based shifts, are also underway and may eventually be incorporated into the pipeline as well as the IRAF/STSDAS off-line version. We expect that the inclusion of MultiDrizzle in the Hubble archive pipelines and its delivery to the community represents a significant milestone in enhancing the scientific quality of Hubble archive pipeline products.

Acknowledgements:

Many thanks to Andy Fruchter, Chris Hanley, Warren Hack, Richard Hook, and Robert Jedrzejewski for code development and concepts; Shireen Gonzaga, Vera Platais-Kozhurina, Linda Dressel, Eddie Bergeron, Max Mutchler and Jennifer Mack for extensive testing, and the STScI Dither Group for additional support and discussions.

References:

- *Fruchter, A. S & Hook, R. N. 2002, PASP 114, 144*
- *Koekemoer, A. M., Fruchter, A. S., Hook, R. N., & Hack, W. 2002, HST Calibration Workshop, ed. S. Arribas, A. M. Koekemoer, & B. Whitmore (STScI: Baltimore), 337*
- *Koekemoer, A. M. et al. 2005, HST Dither Handbook, V3.0 (STScI: Baltimore)*

Hubble captures Deep Impact's collision with a comet

On July 4th at 7:52 CEST an extraordinary event took place some 130 million kilometres away from the Earth. A 370-kilogram copper projectile released by NASA's Deep Impact spacecraft plunged into comet 9P/Tempel 1.

From the Earth hundreds of telescopes observed the event both from ground and from space. This series of Hubble images captured the ejection of a bright plume of dust following the July 4th collision. The image sequence dramatically shows the evolution of material that was blasted off the comet as it expands and diffuses into interplanetary space.

The images show the fan-shaped ejecta expanding at 720 kilometres an hour over a 24-hour period following impact. The upper-left image shows the comet some minutes before impact.

The upper centre image shows that just 12 minutes after the collision, the innermost coma of dust appears 10 times brighter than in the pre-impact photo. The impact caused a brilliant flash of light and a constant increase in the brightness of the inner cloud of dust.

The Hubble Space Telescope continued to monitor the comet, snapping another image (upper right) an hour after the encounter. In this photo, the dust ejected during the impact is expanding outward in the shape of a fan. The debris extends about 720 kilometres from the nucleus. This expansion continues through the lower series of photos. In the lower centre photo, the cloud is 3,200 kilometres across. The last picture in the sequence shows the cloud becoming more diffuse.

The potato-shaped comet is about 13 kilometres long and 4 kilometres wide. Tempel 1's nucleus is too small for the Hubble telescope to resolve. Instead, the bright central region is a combination of light reflected from the nucleus and from dust in the immediate region around the nucleus.

At the European Southern Observatory a large observing campaign was planned for the time before, during and after the impact. On the 4th and 5th of July press meetings were held at the ESO Headquarters in Garching, Germany. There were live transmissions between ESA/ESTEC and ESO, and also between ESO's observatories in Chile.

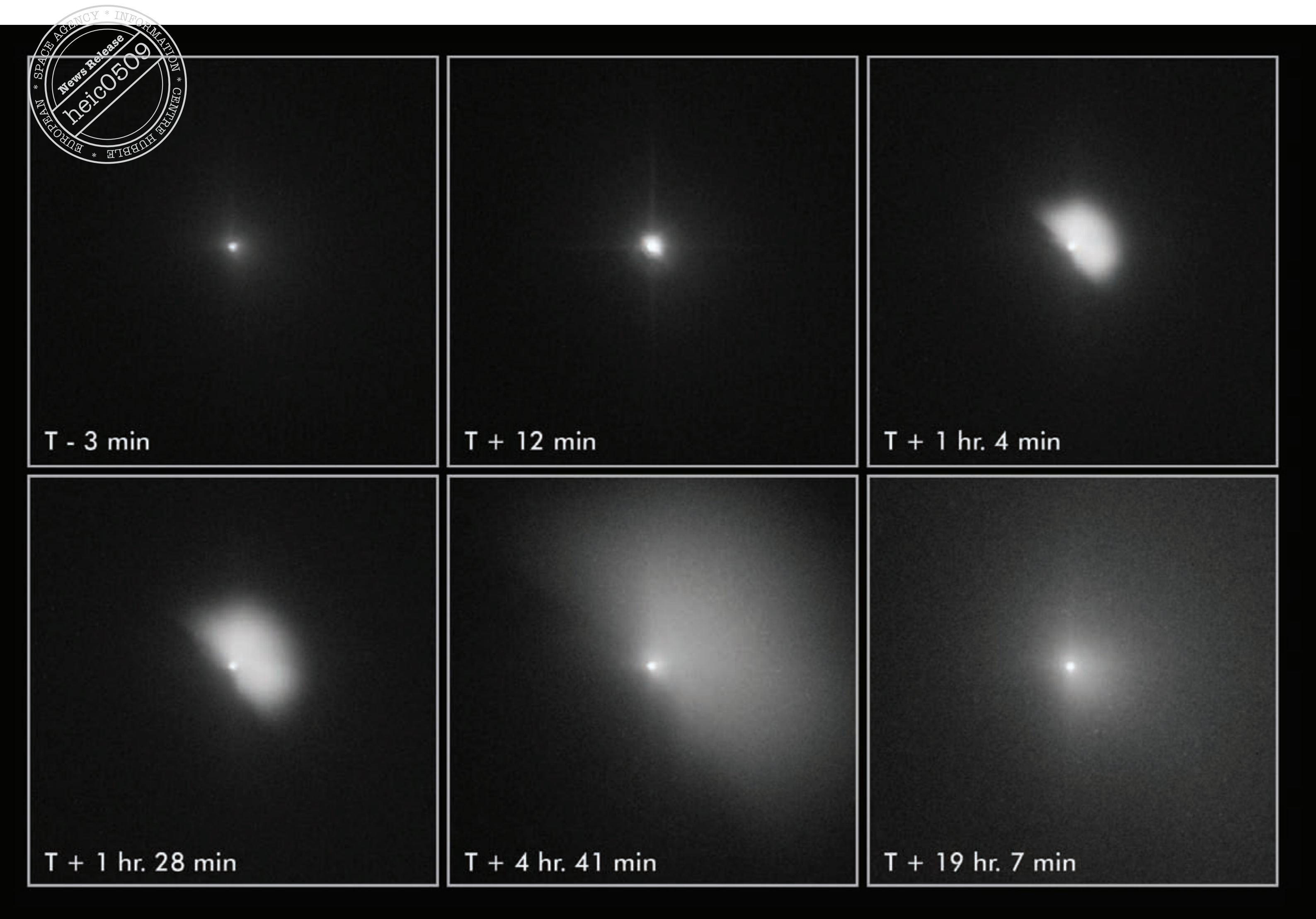

ESA (Artist's impreeion)

An artist's impression showing the Deep Impact spacecraft as it releases the Impactor before its plunge towards comet Tempel 1.

The first Hubble images and movies were published on the web in the afternoon of the 4th of July, less than 10 hours after impact.

Scientists from the ST-ECF took part in the large media attention around the Deep Impact event and gave several interviews to European newspapers, radio and TV.

All in all the Deep Impact event was an impressive example of the fruitful collaboration between scientists, communicators and press, as well as yet another case demonstrating the strong synergy between observatories on the ground and in space.

NASA/JPL-Caltech/UMD

This spectacular image of comet Tempel 1 was taken 67 seconds after it obliterated Deep Impact's impactor spacecraft. The image was taken by the high-resolution camera on the mission's flyby craft iteself. Scattered light from the collision saturated the camera's detector, creating the bright splash seen here. Linear spokes of light radiate away from the impact site, while reflected sunlight illuminates most of the comet surface. The image reveals topographic features, including ridges, scalloped edges and possibly impact craters formed long ago.

NASA, ESA, P. Feldman (Johns Hopkins University) and H. Weaver (Johns Hopkins University Applied Physics Lab)

CONTENTS

The Hubble Anniversary DVD

The cover of the Greek version of the DVD. Greece made a record distribution of 162,000 copies.

ESA's anniversary DVD film "Hubble – 15 years of discovery", supplied with this issue of the ST-ECF Newsletter, covers all aspects of the Hubble Space Telescope project. It is a journey through the history, the troubled early life and the ultimate scientific successes of Hubble. This profile, directed by Lars Lindberg Christensen, contains large amounts of previously unpublished footage of superb quality.

Hubble's spectacular visual images make a stunning backdrop throughout the film, bringing an immediacy and vitality as the narrative reveals the new insights Hubble has inspired in all fields of astronomy from exoplanets to black holes. Complex though the science behind the telescope's images often is, Art Director Martin Kornmesser has developed a unique style of elaborate 3D animation that enhances and vividly clarifies the underlying science. The movie is presented by the head of the ST-ECF and a regular Hubble user, Robert (Bob) Fosbury.

The 83-minute DVD contains more than 60 minutes of bonus material and includes narration in three languages: English, German and Greek. In addition, there are subtitles in 15 languages: Bulgarian, Danish, Dutch, English, Finnish, French, German, Greek, Italian, Norwegian, Polish, Portuguese, Russian, Spanish and Swedish. A future version 2 of the DVD will also contain an Italian narration and an anticipated further 200,000 copies will be distributed.

ST-ECF

Head
Robert A.E. Fosbury
+49-89-320 06 235
Robert.Fosbury@stecf.org

Public Outreach
(Hubble European Space Agency Information Centre):
Lars L. Christensen
+49-89-320 06 306
lars@stecf.org

The Space Telescope-European Coordination Facility
Karl-Schwarzschild-Str.2
D-85748 Garching bei München, Germany

Websites
http://www.stecf.org and http://www.spacetelescope.org

Telephone
+49-89-320 06 291

Telefax
+49-89-320 06 703

Hot-line (email)
stdesk@stecf.org

Email
<user>@stecf.org

ST-ECF Newsletter

Editor
Richard Hook, Richard.Hook@stecf.org

Editorial assistant
Britt Sjöberg, Britt.Sjoeberg@stecf.org

Layout, illustrations and production
Lars L. Christensen & Martin Kornmesser

Printed by
TypeSet, München

Published by
ST-ECF